CALCULATIONS OF PLASMA PARAMETERS FOR HIGH POWER IMPULSE REFLEX DISCHARGE

Yu.V. Kovtun
National Science Center "Kharkov Institute of Physics and Technology", Kharkov, Ukraine
E-mail: Ykovtun@kipt.kharkov.ua

The temporal behavior of the plasma parameters in a high power impulse reflex discharge are investigated using a time dependent global (volume averaged) model. The density of neutral atoms and cathode material ions coming into the discharge by the cathode sputtering mechanism is determined. The comparison between the calculation data and experimental results is provided.

PACS: 52.80.-s; 52.80.Sm

INTRODUCTION

The gas discharge plasma formed in the reflex discharge (Penning discharge) is used in many technical devices which are widely used for solving both physical and applied problems, for example, in the charged particle sources [1], ion pumps and vacuum gauges [2] etc. The reflex discharge was first proposed by Penning F.M. [3] in 1936 for developing a vacuum manometer. During the many-year history a large number of various reflex discharge models were offered and investigated. However, despite the long-term and numerous researches, there is no satisfactorily complete physical model that would describe the reflex discharge. This circumstance is partially connected with the fact that the reflex discharge has a number of modes depending on the working gas pressure and the magnetic field [4]. In the case of low gas pressure ($p \le 1.33 \cdot 10^{-2}$ Pa) in the interelectrode space a negative volume charge is predominant. Under higher gas pressures ($p > 1.33 \cdot 10^{-2}$ Pa) the whole interelectrode space is filled with plasma. The reflex discharge under pressures above $p > 1.33 \cdot 10^{-2}$ Pa is often used as a base for formation of plasma sources.

Global (volume-averaged) models of steady-state and pulse plasma discharges [5] are simple but rather powerful tools to analyze. They have less computational load and results of simulation can be analyzed relatively easily. In [6], a model of stationary reflex discharge on the basis of the volume-averaged (global) model [5, 7] was proposed and analyzed. The difference between experimental results with calculated data in [6] was within a factor ~2. The model proposed in [6] was further developed in [8]. The model takes into account the Penning ionization of sputtered cathode atoms and their influence on the balance of charged particles in plasma.

The authors of [9] investigated the behaviour of argon plasmas produced by time-modulated power in high-density plasma reactors using a spatially averaged (global) model. A global plasma model for an ionized physical vapor deposition (IPVD) system is described in [10]. The ionization mechanism and the temporal behavior of the plasma parameters in a high power impulse magnetron sputtering (HiPIMS) discharge was investigated in [11] using a time dependent global model. A time-dependent global plasma model for ionization region (IRM model) in a HiPIMS discharge was proposed and analyzed in [12]. The processes of modulated pulsed power magnetron sputtering (MPPMS) discharge are numerically modeled (time-dependent global plasma model) and experimentally investigated in [13].

The previous experience [14, 15] testifies that the high power impulse reflex discharge is an effective instrument for producing a multicomponent gas-metal plasma. In this case, the metal plasma component is formed as a result of the ionization of particles sputtered from cathode that penetrate into the discharge. The processes of injection of a sputtered and ionized working material into the impulse reflex discharge plasma have been considered in [16] at an initial stage of dense gas-metal plasma formation. A calculation model has been proposed to estimate the parameters of the sputtering mechanism for the required working material to be injected into the discharge.

In the present paper the modeling of a high power impulse reflex discharge is provided on the base of the time dependent global (volume-averaged) model.

1. EXPERIMENTAL DETAILS

The parameters of the multicomponent gas-metal plasma of a high-power impulse reflex discharge were investigated at the "MAKET" facility [14] representing the stainless steel vacuum chamber with the internal diameter of 20 cm and the length of 200 cm. A maximum magnetic field induction is $B_0 \le 0.9$ T, magnetic field pulse duration – 18 ms. The vacuum chamber was pumped down to a pressure of $1.33 \cdot 10^{-4}$ Pa; then the igniting gas Ar was let into the chamber. The plasma was produced by discharging a capacitor bank (C = 560 μF, U_0 = 3.8 kV) between two cold cathodes with diameter Ø = 10 cm, and the anode (vacuum chamber). The cathodes were made from metallic Ti. The gas–metal plasma was produced in the mixture of the igniter gas and the sputtered cathode material.

The multicomponent gas-metal plasma density was investigated by microwave interferometry method. The plasma probing was performed across the plasma column using the ordinary O-wave with the wavelengths λ = 8 mm and λ = 4.13 mm. Besides, the current-voltage characteristic of the discharge was regularly measured, giving possibility to estimate the energy deposited in plasma.

2. THE PULSED-POWER MODEL

The calculation is done by utilizing a time dependent global model of a cylindrical plasma discharge, assuming uniform spatial distributions of plasma parameters over the plasma volume. All species densities are volume averaged. The electron density N_e is directly given by the ion densities N_i assuming quasineutrality of the plasma $N_e = \Sigma Z_i N_i$, where Z_i is ion charge. In the reflex

discharge the most part of electrons go away in the radial direction to the anode, and ions are axially directed to the cathodes. The fluxes of ions and electrons are assumed to be equal. The electrons are assumed to be in thermal equilibrium and have a Maxwellian-like energy distribution function.

The total heat balance of the rotating plasma was considered in [17, 18] with assumption that the power is deposited uniformly into the plasma volume. The absorbed power was assumed equals to $P_{abs}(t) = P_d(t)F_d$, where $P_d(t)$ is discharge power input, $P_d(t) = I_d(t)\,U_d(t)$, and F_d is the adjustable parameter. The discharge voltage $U_d(t)$ and the discharge current $I_d(t)$ were determined experimentally. A fitting parameter F_d represents the fraction of the discharge power input that goes into heating of electrons. In the paper [18] the components of the energy balance in rotating plasma were calculated. Taking into account the results of [18], the adjustable parameter was taken as $F_d = 0.35$. The plasma is described by a set of nonlinear equations: particle balance equation for each of the species and one power balance equation were calculated in sections 3 and 4.

3. PARTICLE BALANCE

In generalized form, the particle balance equation is given by:

$$\frac{dN}{dt} = \sum_i R_{\text{Gener, i}} - \sum_i R_{\text{Loss, i}}\,, \qquad (1)$$

where $R_{\text{Gener,i}}$ and $R_{\text{Loss,i}}$ are the characteristic particle generation rate and loss rate, respectively, with including of variety of processes running in plasma – such as ionization, excitation, recombination, diffusion, charge exchange, and others.

3.1. PARTICLE BALANCE FOR Ar SPECIES

The rate equation for the working gas Ar is

$$\begin{aligned}\frac{dN_{\text{Ar}}}{dt} &= \frac{1}{V_p}\left(N_{\text{Ar}^+}\nu_B^{\text{Ar}^+}A_{\text{eff}} + N_{\text{Ar}^{2+}}\nu_B^{\text{Ar}^{2+}}A_{\text{eff}}\right)+\\ &+ N_{\text{Ar}^+}\left(N_e\left(N_e\alpha_3 + \alpha_{\text{RR}} + N_{\text{Ar}}\alpha_{\text{tb}} + \alpha_{\text{DR}}\right) + N_{\text{Ti}}K_{\text{CT}}^{\text{Ar}^+-\text{Ti}}\right)-\\ &- N_{\text{Ar}}\left(N_eK_{\text{iz}}^{\text{Ar}} + N_{\text{Ar}^{2+}}K_{\text{CT}}^{\text{Ar}^{2+}-\text{Ar}}\right),\end{aligned} \qquad (2)$$

where N_{Ar}, N_{Ti}, $N_{\text{Ar}}{}^+$, $N_{\text{Ar}}{}^{2+}$, N_e are densities of: neutral atoms Ar and Ti, ions Ar^+ and Ar^{2+}, electrons; $\nu_B^{\text{Ar}^+}$, $\nu_B^{\text{Ar}^{2+}}$ the Bohm velocity of ions Ar^+ and Ar^{2+}; $K_{\text{CT}}^{\text{Ar}^+-\text{Ti}}$, $K_{\text{CT}}^{\text{Ar}^{2+}-\text{Ar}}$ are the rate constants of gas ion charge transfer; V_p – the plasma volume; A_{eff} is the effective area for charged particle loss; $K_{\text{iz}}^{\text{Ar}}$ is the rate constant for the neutral particle ionization; α_3 – the rate constant for the collisional three-body (e – e – ion) recombination; α_{tb} – the rate constant for the collisional three-body (e – neutral – ion) recombination; α_{RR} – the rate constant for the electron-ion radiative recombination; α_{RD} – the rate constant for the dielectronic recombination.

For Ar^+ ions the rate equation can be written as

$$\begin{aligned}\frac{dN_{\text{Ar}^+}}{dt} &= N_{\text{Ar}}N_eK_{\text{iz}}^{\text{Ar}} + N_{\text{Ar}^{2+}}\left(N_e\left(N_e\alpha_3^1 + \alpha_{\text{RR}}^1 + \alpha_{\text{DR}}^1\right)+\right.\\ &\left.+ 2N_{\text{Ar}}K_{\text{CT}}^{\text{Ar}^{2+}-\text{Ar}}\right) - N_{\text{Ar}^+}\left(N_e\left(N_e\alpha_3 + \alpha_{\text{RR}} + N_{\text{Ar}}\alpha_{\text{tb}} + \alpha_{\text{DR}}\right.\right.\\ &\left.\left.+ K_{\text{iz}}^{\text{Ar}^+}\right) + N_{\text{Ti}}K_{\text{CT}}^{\text{Ar}^+-\text{Ti}}\right) - N_{\text{Ar}^+}N_eK_{\text{iz}}^{\text{Ar}^+} - \frac{1}{V_p}N_{\text{Ar}^+}\nu_B^{\text{Ar}^+}A_{\text{eff}}\,,\end{aligned} \qquad (3)$$

where $\alpha_3{}^1$; $\alpha_{\text{RR}}{}^1$ $\alpha_{\text{RD}}{}^1$ are the rate constants for recombination of Ar^{2+} ions ; $K_{\text{iz}}^{\text{Ar}^+}$ is the rate constant for the ionization ion Ar^+.

The rate equation for Ar^{2+} ions is

$$\begin{aligned}\frac{dN_{\text{Ar}^{2+}}}{dt} &= N_{\text{Ar}^+}N_eK_{\text{iz}}^{\text{Ar}^+} - N_{\text{Ar}^{2+}}\left(N_e\left(N_e\alpha_3^1 + \alpha_{\text{RR}}^1 + \alpha_{\text{DR}}^1\right)+\right.\\ &\left.+ N_{\text{Ar}}K_{\text{CT}}^{\text{Ar}^{2+}-\text{Ar}}\right) - \frac{1}{V_p}N_{\text{Ar}^{2+}}\nu_B^{\text{Ar}^{2+}}A_{\text{eff}}\,.\end{aligned} \qquad (4)$$

The rate constants, cross-sections, and various process parameters used in the calculations were taken from [19 - 28]. They are quoted in Table.

3.2. PARTICLE BALANCE FOR Ti SPECIES

The interaction of plasma formed in the reflex discharge with the cathode surface results in destruction of a cathode material owing to sputtering; the eroded material goes into the plasma and is subsequently ionized.

The rate equation for Ti atoms is:

$$\begin{aligned}\frac{dN_{\text{Ti}}}{dt} &= \frac{1}{V_p}\left(\text{Y}_gN_{\text{Ar}^+}\nu_B^{\text{Ar}^+}A^1_{\text{eff}} + \text{Y}_gN_{\text{Ar}^{2+}}\nu_B^{\text{Ar}^{2+}}A^1_{\text{eff}} +\right.\\ &+ \text{Y}_mN_{\text{Ti}^+}\nu_B^{\text{Ti}^+}A^1_{\text{eff}} + \text{Y}_mN_{\text{Ti}^{2+}}\nu_B^{\text{Ti}^{2+}}A^1_{\text{eff}} +\\ &\left.+ \text{Y}_mN_{\text{Ti}^{3+}}\nu_B^{\text{Ti}^{3+}}A^1_{\text{eff}}\right) + N_{\text{Ti}^+}\left(N_e\left(N_e\alpha^{11}{}_3 + \alpha^{11}{}_{\text{RR}} + \alpha^{11}{}_{\text{DR}}\right)\right) -\\ &- N_{\text{Ar}^+}N_{\text{Ti}}K_{\text{CT}}^{\text{Ar}^+-\text{Ti}} - N_{\text{Ti}}N_eK_{\text{iz}}^{\text{Ti}} - \frac{N_{\text{Ti}}}{\tau_D}\,,\end{aligned} \qquad (5)$$

Here $N_{\text{Ti}}{}^+$, $N_{\text{Ti}}{}^{2+}$, $N_{\text{Ti}}{}^{3+}$ are, respectively, density of ions Ti^+, Ti^{2+} and Ti^{3+}; $\nu_B^{\text{Ti}^+}$, $\nu_B^{\text{Ti}^{2+}}$, $\nu_B^{\text{Ti}^{3+}}$ are Bohm velocity of ions Ti^+, Ti^{2+} and Ti^{3+}; K_{iz}^{Ti} is the rate constant for the neutral particle ionization; $\alpha_3{}^{11}$; $\alpha_{\text{RR}}{}^{11}$, and $\alpha_{\text{RD}}{}^{11}$ are the rate constant for recombination of ion Ti^+; Y_m and Y_g – the sputtering coefficients of the cathode material by metal and gas ions, correspondingly; $A_{\text{eff}}{}^1$ is the effective area of charged particle loss on cathodes; τ_D – the characteristic diffusion time of a sputtered particle, $\tau_D = \Lambda/D_m$, with Λ as the characteristic time of sputtered particle diffusion and D_m – as its diffusion coefficient in the gas or plasma. To calculate the ratio of sputtering, the diffusion time of a neutral atom and the time of its ionization we use the model proposed in [16].

For Ti ions the rate equation can be written as

$$\begin{aligned}\frac{dN_{\text{Ti}^+}}{dt} &= N_{\text{Ti}}N_eK_{\text{iz}}^{\text{Ti}} + N_{\text{Ar}^+}N_{\text{Ti}}K_{\text{CT}}^{\text{Ar}^+-\text{Ti}} +\\ &+ N_{\text{Ti}^{2+}}N_e\left(\alpha^{21}{}_{\text{RR}} + \alpha^{21}{}_{\text{DR}}\right) - N_{\text{Ti}^+}N_eK_{\text{iz}}^{\text{Ti}^+} -\\ &- N_{\text{Ti}^+}\left(N_e\left(N_e\alpha^{11}{}_3 + \alpha^{11}{}_{\text{RR}} + \alpha^{11}{}_{\text{DR}}\right)\right) - \frac{1}{V_p}N_{\text{Ti}^+}\nu_B^{\text{Ti}^+}A_{\text{eff}}\,,\end{aligned} \qquad (6)$$

where $\alpha_{\text{RR}}{}^{21}$, $\alpha_{\text{RD}}{}^{21}$ are the rate constants for recombination of Ti^{2+}; $K_{\text{iz}}^{\text{Ti}^+}$ the rate constant for ionization ion Ti^+.

$$\begin{aligned}\frac{dN_{\text{Ti}^{2+}}}{dt} &= N_{\text{Ti}^+}N_eK_{\text{iz}}^{\text{Ti}^+} + N_{\text{Ti}^{3+}}N_e\left(\alpha^{31}{}_{\text{RR}} + \alpha^{31}{}_{\text{DR}}\right)+\\ &- N_{\text{Ti}^{2+}}N_eK_{\text{iz}}^{\text{Ti}^{2+}} - N_{\text{Ti}^{2+}}N_e\left(\alpha^{21}{}_{\text{RR}} + \alpha^{21}{}_{\text{DR}}\right) - \frac{1}{V_p}N_{\text{Ti}^{2+}}\nu_B^{\text{Ti}^{2+}}A_{\text{eff}}\,,\end{aligned} \qquad (7)$$

The $\alpha_{\text{RR}}{}^{31}$, $\alpha_{\text{RD}}{}^{31}$ are rate constants for recombination of ion Ti^{3+}; $K_{\text{iz}}^{\text{Ti}^{2+}}$ – the rate constant for ionization of ion Ti^{2+}.

$$\frac{dN_{\mathrm{Ti}^{3+}}}{dt} = N_{\mathrm{Ti}^{2+}} N_e K_{iz}^{\mathrm{Ti}^{2+}} - N_{\mathrm{Ti}^{3+}} N_e \left(\alpha^{31}{}_{RR} + \alpha^{31}{}_{DR}\right) - \\ - \frac{1}{V_p} N_{\mathrm{Ti}^{3+}} \nu_B^{\mathrm{Ti}^{3+}} A_{eff}. \quad (8)$$

Process		Rate coefficient	Citation
Ionization			
1	$e + Ar \rightarrow Ar^+ + 2e$	K_{iz}^{Ar}	19
2	$e + Ar^+ \rightarrow Ar^{2+} + 2e$	$K_{iz}^{Ar^+}$	19
3	$e + Ti \rightarrow Ti^+ + 2e$	K_{iz}^{Ti}	19
4	$e + Ti^+ \rightarrow Ti^{2+} + 2e$	$K_{iz}^{Ti^+}$	19
5	$e + Ti^{2+} \rightarrow Ti^{3+} + 2e$	$K_{iz}^{Ti^{2+}}$	19
Three-body recombination			
6	$2e + Ar^+ \rightarrow Ar + e$	α_3	20
7	$2e + Ar^{2+} \rightarrow Ar^+ + e$	$\alpha_3{}^1$	21
8	$Ar^+ + Ar + e \rightarrow Ar + Ar$	α_{tb}	22
9	$2e + Ti^+ \rightarrow Ti + e$	$\alpha_3{}^{11}$	23
Radiative recombination			
10	$e + Ar^+ \rightarrow Ar + h\nu$	α_{RR}	24
11	$e + Ar^{2+} \rightarrow Ar^+ + h\nu$	$\alpha_{RR}{}^1$	24
12	$e + Ti^+ \rightarrow Ti + h\nu$	$\alpha_{RR}{}^{11}$	23
13	$e + Ti^{2+} \rightarrow Ti^{i+} + h\nu$	$\alpha_{RR}{}^{21}$	23
14	$e + Ti^{3+} \rightarrow Ti^{2+} + h\nu$	$\alpha_{RR}{}^{31}$	23
Dielectronic recombination			
15	$e + Ar^+ \rightarrow Ar^* \rightarrow Ar$	α_{RD}	25
16	$e + Ar^{2+} \rightarrow Ar^{+*} \rightarrow Ar^+$	$\alpha_{RD}{}^1$	25
17	$e + Ti^+ \rightarrow Ti^* \rightarrow Ti$	$\alpha_{RD}{}^{11}$	25
18	$e + Ti^{2+} \rightarrow Ti^{+*} \rightarrow Ti^+$	$\alpha_{RD}{}^{21}$	25
19	$e + Ti^{3+} \rightarrow Ti^{2+*} \rightarrow Ti^2$	$\alpha_{RD}{}^{31}$	25
Charge transfer			
20	$Ar + Ar^{2+} \rightarrow Ar^+ + Ar^+$	$K_{CT}^{Ar^{2+}-Ar}$	26
21	$Ti + Ar^+ \rightarrow Ti^+ + Ar$	$K_{CT}^{Ar^+-Ti}$	27
Sputtering			
22	$Ar^+ \rightarrow Ti$	Y_g	28
23	$Ar^{2+} \rightarrow Ti$	Y_g	28
24	$Ti^+ \rightarrow Ti$	Y_m	28
25	$Ti^{2+} \rightarrow Ti$	Y_m	28
26	$Ti^{3+} \rightarrow Ti$	Y_m	28

* excited atoms and ions

3.3. PARTICLE BALANCE FOR ELECTRONS

The continuity equation for the electrons is determined by quasineutrality, the electron flux across the boundary is obtained as the sum of all ion fluxes. Accordingly, for equation 1, the characteristic rates of generation and loss of electrons are similar to those described in equations 2-8.

4. POWER BALANCE

In the power balance equation the absorbed power equates to power losses. The time-dependent electron temperature T_e can be obtained by solving the energy balance equation of the system:

$$V_p \left(\frac{d}{dt} \left(\frac{3}{2} \cdot q \cdot N_e \cdot T_e \right) \right) = P_{abs}(t) - P_{loss}(t), \quad (9)$$

Here P_{abs} is the absorbed power, $P_{abs}(t) = P_d(t) F_d$; $P_{loss}(t)$ – power losses defined as

$$P_{los} = P_{Ve} + P_{le} + P_{li} + P_R + P_{ll}, \quad (10)$$

where P_{Ve} is the power released in the volume due to energy loss in collisions of electron with neutral particles; P_{le} is plasma power taken by electrons; P_{li} – plasma power taken by ions; P_R – power of recombination (free-bound) radiation [23]; P_{ll} – power lost in electron-ion collisions.

A part of the input power is also lost as kinetic energy loss of particles (electrons and ions) to the walls, what can be described as

$$P_{le} = q \cdot N_e \cdot \nu_B \cdot A_{eff} \cdot W_e, \quad (11)$$

$$P_{li} = \Sigma\, q \cdot Z_i \cdot N_i \cdot \nu_B \cdot A_{eff} \cdot W_i. \quad (12)$$

In these equations q is electron charge; W_e – the average kinetic energy taken by electrons, in the Maxwell distribution assumption its value is $2T_e$; W_i – average kinetic energy taken by ions, which equals to the sum of ion energies before coming into the sheath (Debye sheath) and obtained in the sheath, $W_i = (T_e/2) + V_s$, where V_s is the cathode potential drop approximately equals to the discharge voltage U_d.

The power lost in electron-ion collisions is defined according to:

$$P_{ll} = V_p \Sigma\, q \cdot Z_i \cdot N_i \cdot (3\, m_e / m_i) \cdot (T_e - T_g) \cdot W_i \cdot \nu_{ei}. \quad (13)$$

Here m_e and m_i are mass of electron and ion; ν_{ei} – is the electron-ion collision rate, T_g is the gas temperature.

The power released in the volume due to the electron energy loss during collision with neutral particles defined as:

$$P_{Ve} = q \cdot N_e \cdot N_0 \cdot V_p \cdot W_{iz} \cdot K_{iz}. \quad (14)$$

For ions this equation takes the form:

$$P_{Ve} = \Sigma\, q \cdot N_e \cdot N_0 \cdot V_p \cdot W_{iz} \cdot K_{iz}, \quad (15)$$

where W_{iz} is the average energy spent for ion-electron pair formation or the ionization cost. For neutral titanium and ions (Ar^+, Ti^+, Ti^{2+}, Ti^{3+}), the value W_{iz} was taken equal to the ionization potential.

4.1. MEAN ENERGY EXPENDED PER ION PAIR BY ELECTRONS

For partly ionized plasma, it is necessary to take into account all processes associated with direct, cascade, and nonradiative transitions, and the ionization cost in this case depends not only on the temperature, but also on the electron number density. The calculations taking into account all the processes are rather complicated. In the model proposed in [7], cascade and nonradiative transitions are ignored. Thus, the mean energy expended per ion pair by electrons for an atom can be determined from the relation [7]:

$$W_{iz}(T_e) = E_{iz} + \sum_i E_{exc,i} \frac{K_{exc,i}(T_e)}{K_{iz}(T_e)} + \\ + \frac{K_{elas}(T_e)}{K_{iz}(T_e)} \frac{3m_e}{m_M} T_e, \quad (16)$$

where $E_{exc,i}$ and $K_{exc,i}$ denote, respectively, the energy and the excitation rate constants of electronic levels of the atom; E_{iz} and K_{iz} are the energy and the rate constant of ionization, K_{elas} is the rate constant of elastic collisions. In the calculations are used the cross sections of the elementary processes: elastic scattering [29], excitation of 43 electron levels of Ar atoms [29, 30], ionization [19]. The results of the calculation are shown in Fig. 1.

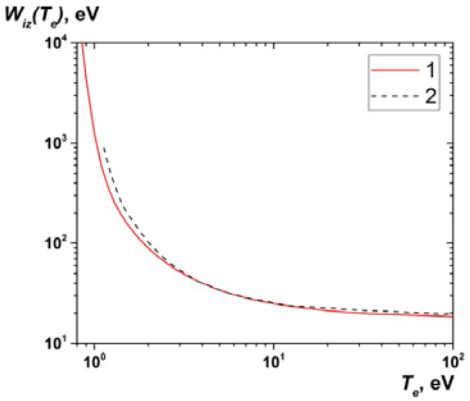

Fig. 1. Mean energy per electron-ion pair for Ar on electron temperature: present results (curve 1), data [31] (curve 2)

5. RESULTS AND DISCUSSION

5.1. CALCULATION RESULTS

Let us calculate the density and electron temperature in the high power impulse reflex discharge. The initial conditions are as follows: plasma column radius $R = 0.1$ m; its length – $L = 1.35$ m; Ar pressure $p = 0.267$ Pa ($N_0 = 7.075 \cdot 10^{19}$ m^{-3}); the plasma volume $V = 0.042$ m^3; cathode surface area – 0.016 m^2, area of the end surface of the plasma cylinder – 0.063 m^2. Initial electron density $N_e = 4 \cdot 10^{16}$ m^{-3}, $T_e = 1$ eV.

A system of 9 ordinary differential equations was solved numerically, using the fourth-order Runge-Kutta fixed-step method. The results of calculations are shown in Figs. 2-4. By convention, the time behavior of the gas-metal plasma density can be divided into three stages. The first stage consists in the plasma creation and its density rise. The second stage presents the existence of the dense highly ionized plasma. The degree of ionization of argon and titanium is, respectively ≈ 84% and ~ 100% (see Fig. 4). The third stage – when plasma density is decreasing and decays. The maximum electron temperature (see Fig. 2,b) was 7 eV (first stage), the minimum 0.38 eV (third stage). The maximum particle density was (see Fig. 3): electrons $N_e = 7.15 \cdot 10^{19}$ m^{-3}; argon ions $5.96 \cdot 10^{19}$ m^{-3} (Ar^+) and $3.3 \cdot 10^{17}$ m^{-3} (Ar^{2+}); titanium ions $4.43 \cdot 10^{17}$ m^{-3} (Ti^+), $1.33 \cdot 10^{18}$ m^{-3} (Ti^{2+}) and $3.29 \cdot 10^{16}$ m^{-3} (Ti^{3+}). The density of titanium ions Ti^{2+} is greater than that of ions Ti^+. In Penning-type plasma source [32], the density of Ti^{2+} is less than that of Ti^+. This is due to the failure to take into account a number of elementary processes, the cross sections of which are absent in the literature.

These are the processes: of charge transfer (Ti, Ar – neutral atoms, Ar^* – excited atoms, Ar^m – metastable atoms)

$$Ti^{2+} + Ti \rightarrow Ti^+ + Ti^+, \quad (17)$$
$$Ti^{2+} + Ar \rightarrow Ti^+ + Ar^+, \quad (18)$$
$$Ti^{2+} + Ar^* \rightarrow Ti^+ + Ar^+, \quad (19)$$
$$Ti^{2+} + Ar^m \rightarrow Ti^+ + Ar^+, \quad (20)$$

and three-body recombination

$$2e + Ti^{2+} \rightarrow Ti^+ + e, \quad (21)$$
$$Ti^{2+} + Ti + e \rightarrow Ti^+ + Ti, \quad (22)$$
$$Ti^{2+} + Ar + e \rightarrow Ti^+ + Ar. \quad (23)$$

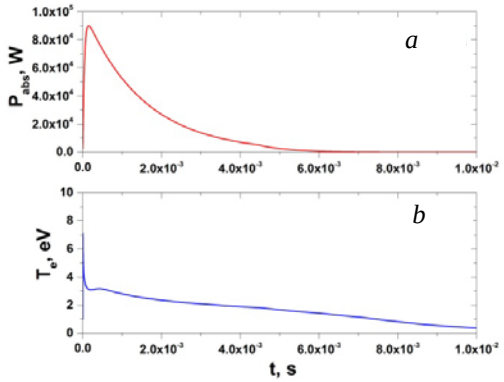

Fig. 2. Modeled time evolution of the adsorbed power P_{abs} (a) and electron temperatures (b)

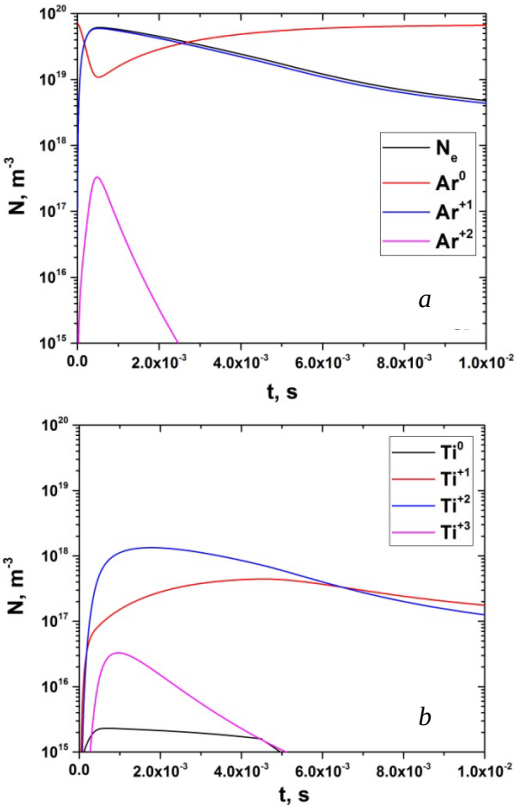

Fig. 3. Modeled time evolution of the density of electrons, argon atoms, species ions (a) and titan atoms, species ions (b)

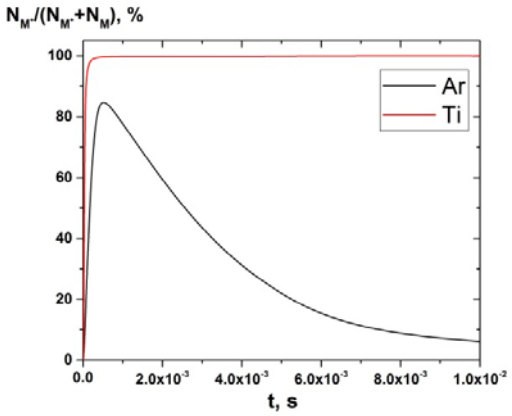

Fig. 4. Degree of ionization of Ar atoms, and sputtered metal (Ti) atoms

The density of neutral argon atoms is greater than of titanium. Accordingly, the reactions (18) - (20), (23) with neutral argon will make a significant contribution. Pro-

ISSN 1562-6016. ВАНТ. 2018. №4(116)

cess (18) is endothermic, respectively, under the given conditions is unlikely. The lifetime of the excited states of argon atoms is small in comparison with the collision time. Therefore, the contribution of process 19 is apparently insignificant. In contrast, the processes of 20 (the lifetime of metastable levels Ar^m is longer than the collision time), 21, and 23 make the greatest contribution to the decrease of the Ti^{2+} ions charge. In calculations there were not taken into account the concentrations of metastable atoms Ar^m and the dimers (Ar_2^+, $ArTi^+$, Ti_2^+), which can be formed in the discharge plasma [33]. Thus, the decrease of Ti^{2+} ions density (see Fig. 3) can be explained if accounting all processes enumerated above.

5.2. COMPARISON WITH MEASUREMENTS

Fig. 5 shows the comparison of electron density measured in a high-power impulse reflex discharge and that found by calculations (the initial stage of the discharge). As can be seen, the results of the calculations differ from the experimental data by no more than a factor of ~2. Such difference can be the result of some unaccounted factors in the considered model. For example, in the calculations the electron energy distribution function was assumed to be Maxwellian, whereas in reality, several groups of electrons with different energy can exist in plasma of such discharge.

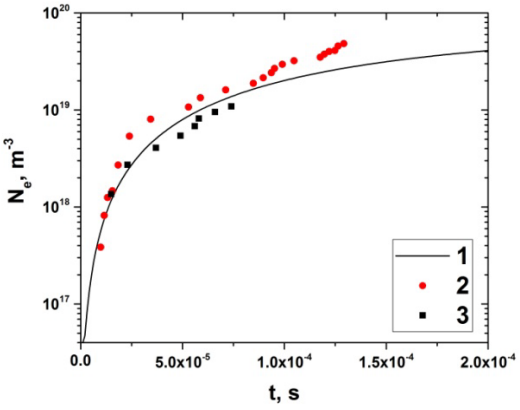

Fig. 5. Comparison of the calculated (1) and experimental (2), (3) electron density at the initial stage of the discharge. Microwave interferometer λ = 4.13 mm (2) and λ = 8 mm (3) (p = 0.267 Pa, U_0 = 3.8 kV)

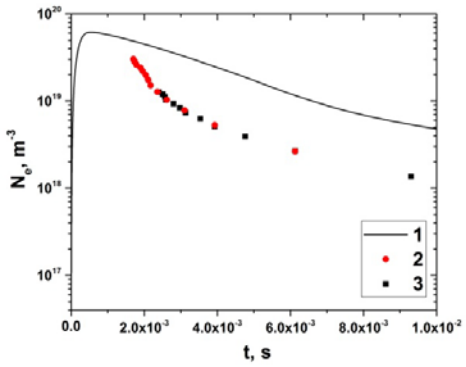

Fig. 6. Comparison of the calculated (1) and experimental (2), (3) electron density. Microwave interferometer λ = 4.13 mm (2) and λ = 8 mm (3) (p = 0.267 Pa, U_0 = 3.8 kV)

During the whole time of the discharge (Fig. 6), the values of calculated and measured electron density differ within factor 2-5: the calculated values are larger than the experimental ones. This fact may be explained by failure to take account of all loss channels for radiative losses and losses of plasma particles. To more fully take into account the radiation losses, it is necessary to create a collisional-radiative plasma model. Besides, classic plasma diffusion across magnetic field was assumed for calculation, but in practice in the reflex discharge an anomalous diffusion with the transverse diffusion coefficient close to the Bohm diffusion coefficient was observed.

CONCLUSIONS

Within the framework of the model under consideration, the plasma density (ions and electrons) and temperature in the high-power impulse reflex discharge are calculated. The processes of cathode material sputtering with subsequent ionization of sputtered atoms in the plasma are investigated. The density of neutral particles and sputtered cathode material atomic ions are determined. The comparison between the calculation data and experimental results has been performed. In general, the modeled densities are in satisfactory agreement with the experimental data. Further development of the model can give more accurate coincidence between the experimental and calculation results.

REFERENCES

1. I.G. Brown. *The Physics and Technology of Ion Sources*. WILEY-VCH Verlag. 2004.
2. N. Yoshimura. *Vacuum Technology*. Springer-Verlag. 2008.
3. F.M. Penning. Ein neues manometer für niedrige gasdrucke, insbesondere zwischen 10^{-3} und 10^{-5} mm // *Physica.* 1937, v. 4, p. 71-75.
4. W. Schuurman. Investigation of a low pressure penning discharge // *Physica.* 1967, v. 36, p. 136-160.
5. M.A. Liberman, A.J. Lichtenberg. *Principles of plasma discharges and materials processing* / John Wiley & Sons, INC Publication, 2005, 757p.
6. Y.V. Kovtun, A.N. Ozerov, A.I. Skibenko, et al. Calculations for parameters of a stationary reflex discharge // *Problems of Atomic Science and Technology. Series «Plasma Physics»*. 2015, № 1(95), p. 201-204.
7. C. Lee, M.A. Lieberman. Global model of Ar, O_2, Cl_2, and Ar/O_2 high density plasma discharges // *J. Vac. Sci. Technol. A.* 1995, v. 13, № 2, p. 368-380.
8. Y.V. Kovtun, A.N. Ozerov, E.I. Skibenko, V.B. Yuferov. Effect of penning ionization on the balance of charged particles in plasma of a stationary reflex discharge // *Ukrain. J. Physics.* 2016, v. 61, p. 702-708.
9. S. Ashida, C. Lee, M.A. Lieberman. Spatially averaged (global) model of time modulated high density argon plasmas // *J. Vac. Sci. Technol. A.* 1995, v. 13, № 5, p. 2498-2507.
10. K. Tao, D. Mao, J. Hopwood. Ionized physical vapor deposition of titanium nitride: A global plasma model // *J. Appl. Phys.* 2002, v. 91, № 7, p. 4040-4048.
11. J.T. Gudmundsson. Ionization mechanism in the high power impulse magnetron sputtering (HiPIMS) discharge // *Journal of Physics: Conference Series.* 2008, v. 100, № 8, p. 082013.

12. M.A. Raadu, I. Axnäs, J.T. Gudmundsson, et al. An ionization region model for high-power impulse magnetron sputtering discharges // *Plasma Sources Science and Technology*. 2011, v. 20, № 6, p. 065007.
13. B.C. Zheng, D. Meng, H.L. Che, M.K. Lei. On the pressure effect in energetic deposition of Cu thin films by modulated pulsed power magnetron sputtering: A global plasma model and experiments // *Journal of Applied Physics*. 2015, v. 117, № 20, p. 203302.
14. Yu.V. Kovtun. Features of Dense Plasma Formation in the Reflex Discharge on Gas-Metal Mixes // *Problems of Atomic Science and Technology. Series «Plasma Electronics and New Methods of Acceleration»*. 2013, № 4, p. 38-43.
15. Y.V. Kovtun, E.I. Skibenko, A.I. Skibenko, et al. Mass distribution of sputtered cathode material in the reflex discharge along the magnetic field mirror configuration // *Problems of Atomic Science and Technology. Series "Plasma Physics"*. 2016, № 1, p. 92-98.
16. Y.V. Kovtun, E.I. Skibenko, A.I. Skibenko, V.B. Yuferov. Estimation of the Efficiency of Material Injection into the Reflex Discharge by Sputtering the Cathode Material // *Ukrainian Journal of Physics*. 2012, v. 57, № 9, p. 901-908.
17. B. Lehnert. Rotating plasmas // *Nuclear Fusion*. 1971, v. 11, № 5, p. 485-533.
18. V.N. Kharchenko, N.P. Poluektov, V.N. Zverev. Peculiarities of heat and mass transfer and magnetohydrodynamic Processes Under pulse ionized gas rotation // *Experimental Thermal and Fluid Science*. 1990, v. 3, № 6, p. 567-573.
19. M. Mattioli, G. Mazzitelli, M. Finkenthal, et al. Updating of ionization data for ionization balance evaluations of atoms and ions for the elements hydrogen to germanium // *Journal of Physics B: Atomic, Molecular and Optical Physics*. 2007, v. 40, № 18, p. 3569-3599.
20. N.A. Dyatko, Y.Z. Ionikh, I.V. Kochetov, et al. Experimental and theoretical study of the transition between diffuse and contracted forms of the glow discharge in argon // *Journal of Physics D: Applied Physics*. 2008, v. 41, № 5, p. 055204.
21. A. Bogaerts, R. Gijbels. Role of Ar^{2+} and Ar_2^+ ions in a direct current argon glow discharge: A numerical description // *J. App. Phy*. 1999, v. 86, p. 4124-4133.
22. T.G. Owano, C.H. Kruger, R.A. Beddini. Electron-ion three-body recombination coefficient of argon // *AIAA journal*. 1993, v. 31, № 1, p. 75-82.
23. J.D. Huba. *NRL plasma formulary*. Naval Research Laboratory, 2016, p. 71.
24. J.M. Shull, M. Van Steenberg. The ionization equilibrium of astrophysically abundant elements // *The Astrophysical Journal. Supplement Series*. 1982, v. 48, p. 95-107.
25. Y. Hahn, A.K. Pradhan, H. Tawara, H.L. Zhang. *Photon and Electron Interactions with Atoms, Molecules and Ions. Collisions of Electrons with Atomic Ions.* Springer-Verlag Berlin Heidelberg, 2001, p. 219.
26. F. Howorka. Thermal rate constant for Ar^{++}+ Ar→ $2Ar^+$ // *The Journal of Chemical Physics*. 1977, v. 67, № 6, p. 2919-2920.
27. A. Bogaerts, K. A. Temelkov, N. K. Vuchkov, R. Gijbels. Calculation of rate constants for asymmetric charge transfer, and their effect on relative sensitivity factors in glow discharge mass spectrometry // *Spectrochimica Acta Part B*. 2007, v. 62, № 4, p. 325-336.
28. Y. Yamamura, H. Tawara. Energy dependence of ion-induced sputtering yields from monatomic solids at normal incidence // *Atomic Data and Nuclear Data Tables*. 1996, v. 62, p. 149-253.
29. E. Gargioni, B. Grosswendt. Electron scattering from argon: Data evaluation and consistency // *Reviews of Modern Physics*. 2008, v. 80, № 2, p. 451-480.
30. Yanguas-Gil Ángel, José Cotrino, Luís L. Alves. An update of argon inelastic cross sections for plasma discharges // *Journal of Physics D: Applied Physics*. 2005, v. 38, № 10, p. 1588-1598.
31. J.T. Gudmundsson, D. Lundin, N. Brenning, et al. An ionization region model of the reactive Ar/O_2 high power impulse magnetron sputtering discharge // *Plasma Sources Science and Technology*. 2016, v. 25, № 6, p. 065004.
32. K. Yukimura, A.P. Ehiasarian, H. Ogiso, et al. Metal ionization in a high-power pulsed sputtering penning discharge // *IEEE Transactions on Plasma Science*. 2011, v. 39, № 11, p. 3125-3132.
33. R. Hippler, M. Cada, V. Stranak, et al. Pressure dependence of Ar_2^+, $ArTi^+$, and Ti_2^+ dimer formation in a magnetron sputtering discharge // *Journal of Physics D: Applied Physics*. 2017, v. 50, № 44, p. 445205.

Article received 13.06.2018

РАСЧЕТ ПАРАМЕТРОВ ПЛАЗМЫ МОЩНОГО ИМПУЛЬСНОГО ОТРАЖАТЕЛЬНОГО РАЗРЯДА

Ю.В. Ковтун

Исследовано изменение параметров плазмы во времени в мощном импульсном отражательном разряде с использованием зависящей от времени глобальной (усредненной по объему) модели. Определена плотность нейтральных атомов и ионов материала катода, поступающих в разряд за счет механизма катодного распыления. Проведено сравнение расчетных данных с результатами эксперимента.

РОЗРАХУНОК ПАРАМЕТРІВ ПЛАЗМИ ПОТУЖНОГО ІМПУЛЬСНОГО ВІДБИВНОГО РОЗРЯДУ

Ю.В. Ковтун

Досліджено зміну параметрів плазми в часі в потужному імпульсному відбивному розряді з використанням залежної від часу глобальної (усередненої за об'ємом) моделі. Визначена густина нейтральних атомів та іонів матеріалу катода, що надходять у розряд за рахунок механізму катодного розпилення. Проведено порівняння розрахункових даних з результатами експерименту.